MOLECULAR AND CELLULAR BIOLOGY, Sept. 2011, p. 3603–3615 Vol. 31, No. 17
0270-7306/11/$12.00 doi:10.1128/MCB.01389-10

MICAL-1 Is a Negative Regulator of MST-NDR Kinase Signaling and Apoptosis▽

Yeping Zhou,[1] Youri Adolfs,[1] W. W. M. Pim Pijnappel,[2] Stephen J. Fuller,[3] Roel C. Van der Schors,[4] Ka Wan Li,[4] Peter H. Sugden,[3] August B. Smit,[4] Alexander Hergovich,[5] and R. Jeroen Pasterkamp[1]*

Department of Neuroscience and Pharmacology, Rudolf Magnus Institute of Neuroscience, University Medical Center Utrecht, Universiteitsweg 100, 3584 CG Utrecht, The Netherlands[1]; Netherlands Proteomics Center, Department of Physiological Chemistry, University Medical Center Utrecht, Universiteitsweg 100, 3584 CG Utrecht, The Netherlands[2]; Institute for Cardiovascular and Metabolic Research, School of Biological Sciences, University of Reading, Reading RG6 6BX, United Kingdom[3]; Department of Molecular and Cellular Neurobiology, CNCR, Neuroscience Campus Amsterdam, VU University, De Boelelaan 1085, 1081 HV Amsterdam, The Netherlands[4]; and UCL Cancer Institute, University College London, 72 Huntley Street, London WC1E 6BT, United Kingdom[5]

Received 3 December 2010/Returned for modification 18 January 2011/Accepted 23 June 2011

MICALs (molecules interacting with CasL) are atypical multidomain flavoenzymes with diverse cellular functions. The molecular pathways employed by MICAL proteins to exert their cellular effects remain largely uncharacterized. Via an unbiased proteomics approach, we identify MICAL-1 as a binding partner of NDR (nuclear Dbf2-related) kinases. NDR1/2 kinases are known to mediate apoptosis downstream of the mammalian Ste-20-like kinase MST1, and ablation of NDR1 in mice predisposes the mice to cancer as a result of compromised apoptosis. MST1 phosphorylates NDR1/2 kinases at their hydrophobic motif, thereby facilitating full NDR kinase activity and function. However, if and how this key phosphorylation event is regulated are unknown. Here we show that MICAL-1 interacts with the hydrophobic motif of NDR1/2 and that overexpression or knockdown of MICAL-1 reduces or augments NDR kinase activation or activity, respectively. Surprisingly, MICAL-1 is a phosphoprotein but not an NDR or MST1 substrate. Rather, MICAL-1 competes with MST1 for NDR binding and thereby antagonizes MST1-induced NDR activation. In line with this inhibitory effect, overexpression or knockdown of MICAL-1 inhibits or enhances, respectively, NDR-dependent proapoptotic signaling induced by extrinsic stimuli. Our findings unveil a previously unknown biological role for MICAL-1 in apoptosis and define a novel negative regulatory mechanism of MST-NDR signaling.

Protein kinases are key regulatory enzymes that control important cellular processes such as growth and apoptosis by changing the properties of a substrate through phosphorylation (20). Given the importance of their biological effects, the catalytic activity of protein kinases is stringently controlled, and defects in this spatiotemporal regulation can cause major diseases such as diabetes and cancer (20). The mammalian Ste-20-like kinase MST1 is part of evolutionary conserved signal transduction pathways with functions in different biological processes of cells. In particular, Hippo signaling (the MST1 fly ortholog) has been studied extensively in *Drosophila melanogaster*, revealing that Hippo tumor suppressor cascades are crucial in the regulation of cell death and proliferation (45). More recently, mammalian MST1 was established as a tumor suppressor protein controlling cell proliferation and apoptosis (45). However, despite these important functions, relatively little is known about the regulation of MST1 or its downstream signaling.

Nuclear-Dbf2-related kinase 1 (NDR1; also known as STK38) and NDR2 (STK38L) can be phosphorylated by MST kinases and mediate apoptotic signaling downstream of MST1 (40). NDR kinases belong to the AGC kinase subfamily and control important cellular processes, such as mitotic exit and apoptosis, in different eukaryotic cells ranging from yeast to neurons (12). Ablation of NDR1 in mice predisposes the mice to the development of T cell lymphoma, presumably as a result of compromised apoptosis (4). The regulation of NDR1/2 kinases by MST kinases and other upstream signaling proteins is best understood in mammalian cells. Binding of MOB1A (Mps-one-binder 1A) to the N-terminal region of NDR1/2 stimulates autophosphorylation on the activation segment and activates NDR kinases (3). The human MOB protein family consists of six distinct members with MOB1 being best studied for its putative tumor suppressive functions through the regulation of NDR/LATS kinases. Additional phosphorylation on the C-terminal hydrophobic motif of NDR1/2 by MST kinases is required for full NDR kinase activation (32). It is evident that these different molecular interactions and activating events need to be tightly controlled, as deregulation of members of the MST, NDR, and MOB protein families has been implicated in diseases such as cancer. Intriguingly, another MOB family member, MOB2, competes with MOB1 for NDR1/2 binding at the NDR N-terminal region, thereby negatively regulating NDR1/2 kinase activity and related functions in centrosome duplication and apoptosis (16). However, whether similar sophisticated regulatory mechanisms exist to control the activation of NDR1/2 by MST kinases is unknown.

Here we identify the multidomain flavoprotein monooxygenase MICAL-1 (MICAL stands for molecule interacting

* Corresponding author. Mailing address: Department of Neuroscience and Pharmacology, Rudolf Magnus Institute of Neuroscience, University Medical Center Utrecht, Universiteitsweg 100, 3584 CG Utrecht, The Netherlands. Phone: 31 88 7568831. Fax: 31 887569032. E-mail: r.j.pasterkamp@umcutrecht.nl.

▽ Published ahead of print on 5 July 2011.

with CasL) (37) as an endogenous binding partner of NDR1/2 kinases. Our findings define a previously unknown biological role for MICAL-1 in apoptosis regulation and show that MICAL-1 negatively controls MST1-NDR apoptotic signaling by competing with MST1 for NDR binding, thereby revealing a novel and unique regulatory mechanism of the MST-NDR pathway. This work opens new avenues for the further molecular delineation of MST/NDR functioning in different cell biological processes and in disease.

MATERIALS AND METHODS

Antibodies and reagents. The generation and purification of anti-T444/442-P and anti-S281/282-P antibodies has been described previously (38). Both antibodies were kindly provided by Brian Hemmings (Friedrich Miescher Institute for Biomedical Research [FMI], Basel, Switzerland). It is important to note that the anti-T444-P and anti-S281-P antibodies recognize the phosphorylated forms of both NDR isoforms, NDR1 (T444-P and S281-P) and NDR2 (T442-P and S282-P). A polyclonal rabbit anti-mouse MICAL-1 antibody was generated by immunizing rabbits with a maltose-binding protein (MBP)–mouse MICAL-1 (mMICAL-1) (amino acid 986 to 1048) fusion protein, which was purified from *Escherichia coli* DH5α cells. The specificity of this antibody was confirmed using Western blotting and immunocytochemistry. We used the following commercially available antibodies: anti-Flag (M2; Stratagene), antihemagglutinin (anti-HA) (3F10; Roche), anti-NDR1 (N-14; Santa Cruz), anti-STK38 (NDR1) monoclonal antibody (2G8-1F3; Abnova), CH11 (Millipore), anti-glutathione *S*-transferase (anti-GST) (Cell Signaling), anti-myc (Cell Signaling), anti-green fluorescent protein (anti-GFP) (Invitrogen), anti-V5 (Invitrogen), anti-α-tubulin (Sigma), antiactin (Sigma), anti-cleaved caspase-3 (Cell Signaling), and anti-poly(ADP-ribose) polymerase (anti-PARP) Asp241 (BD Biosciences). Okadaic acid (OA) was purchased from Enzo Life Sciences, and etoposide, tumor necrosis factor alpha (TNF-α), and cycloheximide (CHX) were purchased from Sigma.

Construction of plasmids. Mouse MICAL-1 and NDR1 cDNAs were amplified from embryonic whole-brain cDNA using standard molecular techniques. To construct a mouse MICAL-1-Flag/HA construct for generating stable L cell lines, mouse MICAL-1 cDNA was subcloned into a pBABE-Flag-HA-puromycin destination vector using the Gateway cloning system (Invitrogen). Mouse MICAL-1 cDNA was also subcloned into pRK5-HA and pRK5-myc (N-terminal tags) using SalI and NotI restriction sites, into pEF-His/V5 vector (C-terminal tag) using the Gateway cloning system (Invitrogen), and into pEGFP (EGFP stands for enhanced green fluorescent protein). Truncation mutants of mouse MICAL-1 were cloned via PCR. Individual PCR products were digested with SalI and NotI and cloned into pRK5-HA or pRK5-myc. Mouse MICAL-1 constructs harboring glycine-to-tryptophan mutations (G3/W3) in the first FAD fingerprint were generated in pRK5-myc and pRK5-HA using the QuikChange site-directed mutagenesis kit (Stratagene). A cDNA encoding the C-terminal 315 amino acids of MICAL-1 was subcloned into the pMAL-P2E vector (BioLabs) between KpnI and HindIII sites for protein expression in *E. coli*. Mouse NDR1 was subcloned into pFLAG-CMV4 (Sigma) (CMV stands for cytomegalovirus) using NotI and BamHI restriction sites. Truncation mutants of mouse NDR1 were cloned via PCR. Individual PCR products were digested with NotI and BamHI and cloned into pFLAG-CMV4. Flag-NDR2, GST-NDR2, NDR1-PIFtide, and HA-MST1 have been described before (8, 11). To generate mouse plexinA4Δecto, a region covering amino acids 1209 to 1891 of the mouse plexin A4 coding sequence was PCR amplified and combined with the plexin A4 signal sequence and a myc tag in the pSG5 vector. All constructs were confirmed by sequence analysis.

To knockdown human *MICAL-1* in cells, SMARTpool technology from Dharmacon was used. A mix of ON-TARGETplus small interfering RNAs (siRNAs) directed against sequences UGGAGAACAUUGUGUACUA, CCUCAGGCA CCAUGAAUAA, GAGUCCACGUCUCCGAUUU, and GUACGAGACCU GUAUGAUG (Dharmacon) in human *MICAL-1* was transiently transfected into cells and efficiently reduced *MICAL-1* levels. An ON-TARGETplus nontargeting siRNA pool from Dharmacon served as a control. To knock down mouse MICAL-1 in L cells, a siRNA oligonucleotide against mouse MICAL-1 (CAGGUGCCAUGACUAAGUAUU [Dharmacon]) was transfected using Oligofectamine and shown to specifically reduce MICAL-1 levels. Nontargeting siRNAs (Dharmacon) were used as controls. To knock down NDR1/2 in L cells, a short hairpin RNA (shRNA) vector targeting both NDR1 and NDR2 (38) was transfected using Lipofectamine 2000 (Invitrogen).

Cell culture and transfection. L, Phoenix, HEK293, and COS-7 cells were maintained in high-glucose Dulbecco's modified Eagle's medium (DMEM; GIBCO) supplemented with 10% fetal bovine serum (FBS) (Lonza), penicillin-streptomycin, and L-glutamine (PAA) at 37°C with 5% CO_2. U2OS T-Rex (tetracycline-inducible MST1 knockdown) cells were cultured as described previously (38). To induce tetracycline-controlled transcriptional activation and MST1 knockdown, 5×10^4 cells were plated in one well of a six-well plate and 2 μg/ml tetracycline was supplied to the culture medium. For protein analysis, exponentially growing cells were plated at 3.5×10^4 cells/cm^2 and transfected the next day using Lipofectamine 2000 (Invitrogen) as described by the manufacturer. For COS-7 cell contraction assays or colocalization experiments, 0.5×10^4 COS-7 cells/cm^2 were seeded on glass coverslips and transfected using FuGENE transfection reagent (Roche) according to the manufacturer's instructions. For transfection of MICAL-1 siRNA oligonucleotides, exponentially growing HEK293 cells or L cells were seeded at 5×10^4 per well in a 6-well plate. After overnight culture, cell were washed with Opti-MEM (Invitrogen) and exposed to a mixture of 1 μl oligonucleotides (mix) (from a 20 μM stock) and 3 μl Oligofectamine (Invitrogen) in Opti-MEM. Four hours after transfection, the medium was replaced with standard culture medium, and the cells were incubated at 37°C with 5% CO_2 for another 48 to 72 h. For double-knockdown experiments with both siRNA oligonucleotides (against MICAL-1) and shRNA vector (against NDR1/2), 5×10^4 L cells were plated in a 6-well plate 1 day before transfection of MICAL-1 oligonucleotide using Oligofectamine. After 24 to 48 h in culture, the cells were transfected with shRNA vector by using Lipofectamine 2000 and cultured for another 48 h for further treatment.

Generation of stable cell lines. A mouse MICAL-1 cDNA was introduced by Gateway cloning into a retroviral destination plasmid derived from pBABE-puro (puro stands for puromycin) carrying a C-terminal Flag PreScission HA tag. L cell clones expressing tagged MICAL-1 were obtained by retroviral transduction and puromycin (Clontech) selection. Positive clonal cell lines were identified by immunoblotting using antibodies directed against HA. After puromycin selection, clonal lines were maintained in culture medium containing 7.5 μg/ml puromycin. L cells with integrated empty pBABE-puro plasmid served as a control.

Pulldown from stable cell lines. Mouse cells expressing MICAL-1-Flag/HA (MICAL-1 tagged with Flag or HA) (D1) and control (C0) L cells were cultured in 500-cm^2 plates (Corning) to 90% confluence. Ten plates from each cell line were harvested by scraping the cells after 2 washes with cold phosphate-buffered saline (PBS). The cells were centrifuged at 1,000 rpm for 15 min at 4°C and lysed by Dounce homogenization in 3 ml of hypotonic lysis buffer containing 10 mM HEPES (pH 8.0), 1.5 mM $MgCl_2$, 10 mM KCl, 0.5 mM phenylmethylsulfonyl fluoride (PMSF), 0.5 mM dithiothreitol (DTT), and protease inhibitor cocktail (Sigma). After the cells were centrifuged at 14,000 rpm for 15 min at 4°C, the supernatant was transferred to a clean Falcon tube, and an equal volume of 2× salt buffer containing 30 mM HEPES (pH 8.0), 190 mM KCl, 30 mM NaCl, 40% glycerol, 0.4 mM EDTA, 0.5 mM PMSF, 0.5 mM DTT, and protease inhibitor cocktail (Sigma) was added. After measuring protein concentration, 100 mg protein from each cell line was added to 100 μl prewashed M2 affinity resin (Sigma) and incubated at 4°C for 3 h. The resin was then washed 4 times with washing buffer (BC-150) containing 20 mM HEPES (pH 8.0), 150 mM NaCl, and 0.5 mM PMSF. Between the third and fourth wash, the sample was washed once in washing buffer (BC-300) containing 20 mM HEPES (pH 8.0), 300 mM NaCl, and 0.5 mM PMSF for 10 min. The proteins were eluted with Flag peptide (Sigma) at 16 μg/μl in BC-150 buffer. The eluted proteins were precipitated as described previously (43) and dissolved in 1× NuPAGE LDS sample buffer (Invitrogen). Finally, proteins were separated on a NuPAGE Novex 4 to 12% Bis-Tris gradient gel following the manufacturer's description (Invitrogen). Proteins were stained using the colloidal blue staining kit (Invitrogen) and processed for mass spectrometry. In addition, 1/20 of each sample was loaded on another NuPAGE gel and processed for silver staining. Briefly, the gel was soaked twice in 50% methanol for 15 min and soaked in 5% methanol for 10 min. After 3 rinses in water, the gel was soaked in 10 μM DTT for 20 min, followed by 0.1% $AgNO_3$ for 20 min. The gel was then washed once in water and twice in developer containing 3% sodium carbonate and 0.0185% formaldehyde. The gel was soaked in developer until protein bands appeared. The reaction was stopped with solid citric acid (about 5% [wt/vol]). The gel was washed with water and scanned.

Gel digestion. Separated proteins were digested in the gel by the method of Shevchenko et al. (29). Gel lanes corresponding to the different protein samples were sliced into 10 bands. Each band was cut into 1-mm cubes, washed with nanopure water, and destained (25 mM ammonium bicarbonate and 50% acetonitrile). After three subsequent destaining steps, the bands were dehydrated for 20 min (100% acetonitrile) and dried in a vacuum centrifuge. The pellets were rehydrated in 30 μl trypsin solution (0.02 μg/μl) (Promega) at 4°C for 45 min, followed by the addition of 400 μl of 50 mM ammonium bicarbonate to

cover the gel pieces. After incubating overnight at room temperature, peptides were extracted two times in 50% acetonitrile in 0.1% trifluoroacetic acid (TFA). The sample was dried in a vacuum centrifuge prior to liquid chromatography coupled to matrix-assisted laser desorption ionization mass spectrometry (LC–MALDI-MS) analysis.

NanoLC and MALDI TOF/TOF analysis. Samples were analyzed as described previously (22) with minor modifications. In brief, peptides were separated on a nanocapillary LC (nanoLC) system (LC Packings/Dionex, Sunnyvale, CA) using an analytical capillary C_{18} column (150 mm by 100 μm inner diameter [ID]) at 400 nl/min, using a linear increase in the concentration of acetonitrile from 5 to 50% (vol/vol) in 90 min and to 90% in 10 min. The eluted gradient was mixed with matrix solution (7 mg of recrystallized α-cyanohydroxycinnaminic acid in 1 ml of 50% (vol/vol) acetonitrile, 0.1% (vol/vol) trifluoroacetic acid, 10 mM ammonium dicitrate) and spotted off-line to a stainless steel MALDI plate (Applied Biosystems) to form a predefined 16 by 24 array (384 spots) using a Probot system (LC Packings/Dionex). The mass spectrometric analysis was carried out using a MALDI tandem time of flight (MALDI-TOF/TOF) instrument (4800 Proteomics Analyzer; Applied Biosystems) with reflector positive ion mode. For MS analysis, an *m/z* mass range of 800 to 3,000 was used with 1,250 shots per spectrum. A maximum of 20 precursors per spot with minimum signal/noise ratio of 50 were selected for data-dependent tandem MS (MS/MS) analysis. An 1-kV collision energy was used for collision-induced dissociation (CID), and 2,500 acquisitions were accumulated for each MS/MS spectrum. All analyses were performed using default calibration, and the mass accuracy was calibrated to within 100 ppm using calibration standards (Applied Biosystems) before each run.

Cell contraction assay. COS-7 and L cell contraction assays were performed as described previously (28, 36). In brief, COS-7 or L cells were transfected with different expression plasmids as described above, fixed after 24 h, and immunostained with anti-Flag, anti-HA, anti-myc, or anti-EGFP antibodies to identify transfected cells. Immunofluorescent images were captured of randomly selected cells using a charge-coupled-device (CCD) camera attached to an Axiovert microscope (Zeiss), and cell area was measured using OpenLab software (Improvision) (17). COS-7 cells with a surface area of $\leq$1,600 μm^2 were defined as contracted. L cell contraction was quantified as described previously (36).

Apoptosis assay. Wild-type L cells or stable C0, D1, or D2 L cells were seeded at 1×10^4 cells/cm^2 in a 24-well plate for 24 h and treated with either dimethyl sulfoxide (DMSO) (0.2%) or etoposide (200 μM) in the cell culture medium for 12 h. Transiently transfected L cells (overexpressing MICAL-1, MICAL-1 mutants, or knockdown oligonucleotides/vectors) were treated with etoposide 24 h or 48 h after transfection. L cells were also induced with TNF-α (50 ng/ml) for 6 h in the presence of cycloheximide (10 μg/ml). For Western blotting, cell lysates were prepared in 30 μl of lysis buffer (per well of a 24-well plate). For fluorescence microscopy, the cells were fixed and incubated with anti-cleaved caspase-3 antibody for 1 h at room temperature, followed by several washes and incubation with anti-rabbit antibody–Alexa Fluor 488. Next, the cells were washed and incubated with phalloidin-tetramethyl rhodamine isothiocyanate (TRITC) (Sigma) to visualize cells and cell morphology.

H_2O_2 detection assay. The Amplex red hydrogen peroxide/peroxidase assay kit (Invitrogen) was used to measure hydrogen peroxide production from the purified enzymatic domain of MICAL-1 and from lysates of transfected HEK293 or L cells as described previously (25, 28). For cell lysate experiments, cells from one well of a six-well plate were lysed by sonication in 120 μl buffer containing 20 mM HEPES (pH 7.4), 100 mM NaCl, and 1× EDTA-free protease inhibitor mixture (Roche), and lysates were cleared by centrifugation. Reactions were performed in 100 μl consisting of 50 μl of cell lysate, 200 μM NADPH, Amplex red reagent (10-acetyl-3,7-dihydroxyphenoxazine), and 0.1 U/ml horseradish peroxidase (HRP) in reaction buffer. Absorbance at 560 nm was measured using a Wallac Victor 1420 multilabel counter (PerkinElmer).

In-gel phosphoprotein staining. Proteins in a NuPAGE Bis-Tris gradient gel (Invitrogen) were either Coomassie blue stained or stained with Pro-Q diamond phosphoprotein gel stain (Invitrogen) according to the manufacturer's instructions. In brief, the gel was incubated in fix solution (50% methanol and 10% acetic acid) for 30 min followed by a second overnight incubation. The next day, the gel was washed 3 times in ultrapure water, stained in Pro-Q stain for 90 min in the dark, and destained in a solution containing 20% acetonitrile and 50 mM sodium acetate (pH 4.0). After a brief wash in ultrapure water, the gel was imaged on a FLA-5000 (Fuji Photo Film Co, Ltd.) using excitation at 532 nm and LPG filter.

Western blotting and immunoprecipitation. According to standard protocols, cells were collected by centrifuging at 1,000 rpm for 10 min at 4°C for 10 min, washed in cold PBS, and lysed in lysis buffer containing 20 mM Tris (pH 8.0), 150 mM KCl, 0.1% Triton X-100, and protease inhibitor cocktail (Roche). After centrifugation at 14,000 rpm for 10 min at 4°C, the lysate was transferred to a clean Eppendorf tube and boiled with sample buffer. For immunoprecipitation, the corresponding antibodies were added to each cell lysate and incubated overnight at 4°C. Then prewashed protein A- or G-agarose (Roche) was added to the lysate and incubated for at least 2 h at 4°C. After 4 washes with lysis buffer, proteins were eluted with sample buffer and boiled at 90°C. To analyze proteins from immunoprecipitated (IP) samples or cell lysates, we used SDS-PAGE and transferred proteins to nitrocellulose (Hybond-C Extra; Amersham). Chemiluminescence (Supersignal; Thermo Scientific) was detected by CL-XPosure film (Thermo Scientific) and quantified using ImageJ.

Recombinant protein purification and binding assay. MBP–MICAL-1-C1 (amino acids 734 to 1048) fusion protein was extracted from *E. coli* DH5α cells, and the MICAL-1-C1 fragment was cleaved from the MBP moiety following the instructions of the manufacturer (New England BioLabs). To check the binding of GST-NDR2 to MICAL-1, HA-tagged MICAL-1 (HA-MICAL-1) (HEK293 cells expressed full-length protein) or MICAL-1-C1 were immobilized on anti-HA- or anti-MICAL-1-coupled protein G-agarose beads, respectively, and mixed with 4 μg GST-NDR2. Antibody-coupled beads were used as negative control to examine the nonspecific binding. After 2 h of incubation at 4°C, beads were washed 4 times with lysis buffer and boiled in the presence of sample buffer. The proteins were then subjected to SDS-PAGE and Western blot analysis.

Kinase assays. (i) NDR kinase peptide assay. Flag-tagged NDR1 (Flag-NDR1) was immunoprecipitated from cell lysates expressing Flag-NDR1 alone or in combination with HA-MICAL-1 and assayed for NDR kinase activity in the presence of 1 mM NDR substrate peptide (KKRNRRLSVA), 100 μM [γ-^{32}P]ATP (~1,000 cpm/pmol), and 20 μM ATP in kinase buffer (20 mM Tris [pH 7.5], 10 mM $MgCl_2$, 1 mM benzamidine, 4 μM leupeptin, 3 μM microcystin, 3 mM DTT, 1 μM cyclic AMP-dependent protein kinase inhibitor peptide). The reaction mixture was incubated for 60 min at 30°C and stopped by adding 50 mM EDTA (pH 7.5). The supernatant of the mixture was spotted onto squares of P-81 phosphocellulose paper (Whatman) and washed 4 times with 1% orthophosphoric acid followed by an acetone wash. Radioactivity was measured in a liquid scintillation counter.

(ii) GST-NDR2 kinase assay using HA-MICAL-1 as a substrate. Full-length rat recombinant NDR2 was cloned into pGEX4-T 3′ in frame with GST, expressed in *E. coli* BL21(DE3)(pLysS) cells with 0.03 mM isopropyl-β-D-1-thiogalactopyranoside (IPTG) induction overnight at 25°C, and purified by glutathione-Sepharose affinity chromatography. For *in vitro* kinase assays, 3 μg of GST-NDR2 fusion protein was incubated with immunoprecipitated HA-MICAL-1 in the presence of 100 μM [γ-^{32}P]ATP (~1,000 cpm/pmol) and 20 μM ATP in kinase buffer for 30 min at 30°C. The reaction was stopped by adding SDS sample buffer, and protein phosphorylation was analyzed by SDS-PAGE and subsequent autoradiography.

(iii) *In vitro* phosphorylation with GST-MST1. Recombinant GST-MST1 was obtained from Sigma. To produce immunopurified HA-tagged proteins, COS-7 cells were transfected and processed for immunoprecipitation using anti-HA antibody as described earlier (10). Immunopurified proteins were then washed twice with MST1 kinase buffer (5 mM Tris [pH 7.5], 2.5 mM beta-glycerophosphate, 1 mM EGTA, 1 mM Na_3VO_4, 4 mM $MgCl_2$, 0.1 mM DTT), before incubating at 30°C for 30 min in 20 μl of reaction buffer (5 mM Tris [pH 7.5], 100 μM ATP, 2.5 mM beta-glycerophosphate, 1 mM EGTA, 1 mM Na_3VO_4, 4 mM $MgCl_2$, 0.1 mM DTT, 10 μCi of [γ-^{32}P]ATP [3,000 Ci/mmol; Hartmann Analytic]) in the absence or presence of GST-MST1 (100 ng per reaction mixture). The reactions were stopped by the addition of Laemmli buffer, before the proteins were separated by SDS-PAGE. Subsequently, total proteins were visualized by Coomassie blue staining, the gels were then dried, and phosphorylated proteins were visualized by autoradiography.

RESULTS

Identification of novel MICAL-1-binding partners. MICALs form a recently discovered and unusual family of evolutionary conserved cytoplasmic proteins composed of an enzymatically active flavoenzyme followed by several protein interaction domains or motifs (18). One *MICAL* gene has been identified in *Drosophila* (*Mical*), while humans and mice have three different *MICAL* genes (*MICAL-1*, *MICAL-2*, and *MICAL-3*) (26, 37, 39). Genetic inactivation of *Mical* in fruit flies leads to defects in neural circuit development, myofilament organization, and bristle formation (2, 13, 15, 39). Although *Drosophila*

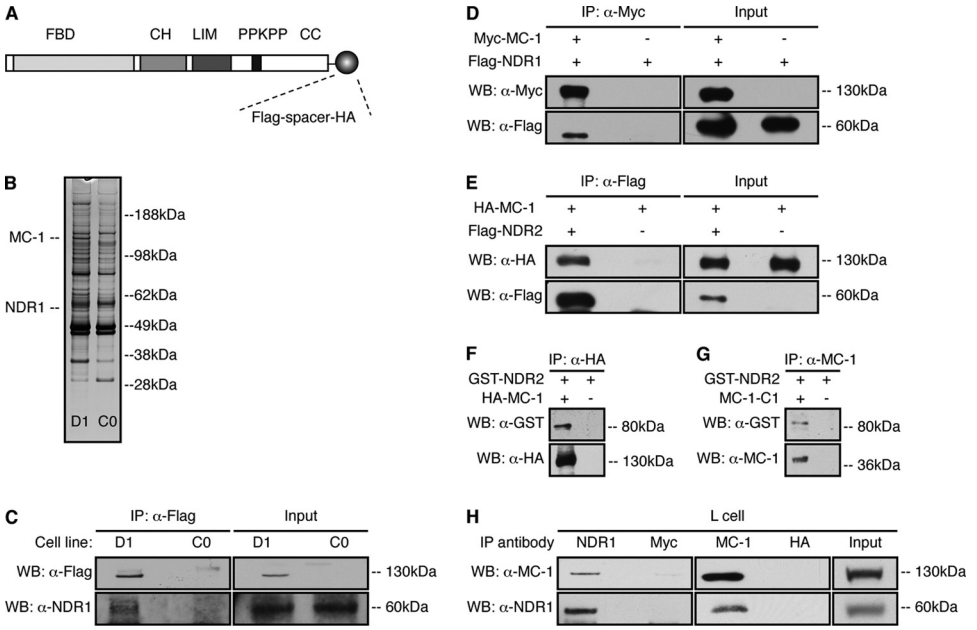

FIG. 1. Mass spectrometry identifies NDR kinases as novel MICAL-1-binding partners. (A) Schematic depicting the domain organization of mouse MICAL-1 fused to the C-terminal Flag and HA epitopes linked by a PreScission sequence (MC-1-Flag/HA). FBD, FAD-binding domain; CH, calponin homology; PPKPP, CasL-binding sequence; CC, coiled-coil. (B) Pulldown assays with anti-Flag monoclonal antibody-conjugated agarose beads were performed on lysates from D1 or C0 cells. Bound proteins were eluted with Flag peptide and analyzed by silver staining. The positions of MICAL-1 and NDR1 on the gel are indicated to the left of the gel. (C) Anti-Flag pulldown assays were performed from D1 and C0 cells as shown in panel B and analyzed by Western blotting (WB) using the indicated antibodies (α-Flag, anti-Flag antibody). IP, immunoprecipitated. (D and E) Lysates from HEK293 cells transfected with epitope-tagged MICAL-1 alone (+) or in combination with Flag-NDR1 (D) or Flag-NDR2 (E) were immunoprecipitated with anti-Myc (D) or anti-Flag (E) antibodies followed by Western blotting. (F and G) Recombinant GST-NDR2 and HA-MICAL-1 purified from HEK293 cells (F) or recombinant MICAL-1-C1 purified from bacteria (G) were mixed and subjected to immunoprecipitation with anti-HA (F) or anti-MICAL-1 (G) antibodies followed by Western blotting with the indicated antibodies. (H) Immunoprecipitation from untransfected L cell extracts followed by Western blotting with the indicated antibodies. Anti-myc and anti-HA antibodies were used as a control for anti-NDR1 and anti-MICAL-1 antibodies, respectively.

Mical has been implicated in the control of F-actin assembly (13), the molecular pathways employed by MICAL proteins to exert their diverse cellular effects remain largely uncharacterized, especially in vertebrate species. To obtain more insight into the MICAL signaling complex and related functions, we used a retroviral vector system to generate L cell lines that stably express a Flag-and-HA-tagged (Flag/HA-tagged) version of mouse MICAL-1 (MICAL-1-Flag/HA) (Fig. 1A), the best-characterized vertebrate MICAL thus far (37). Mouse L cell fibroblasts were used because of their murine origin, their endogenous MICAL-1 expression and the ability of a constitutively active MICAL-1 construct to induce morphological changes in these cells (data not shown). This suggests that L cells contain signaling proteins that are crucial for MICAL-1 function. Clonal cell lines were obtained by retroviral transduction followed by puromycin selection, resulting in several clones expressing MICAL-1-Flag/HA at near endogenous levels. One of these lines (D1) was used for large-scale affinity purification of MICAL-1-Flag/HA complexes followed by silver staining, in-gel tryptic digestion, and mass spectrometry analysis. L cells with integrated empty retroviral vector served as a control (C0) (Fig. 1B). The mass spectrometry analysis identified several proteins that were found in protein complexes from pulldown assays using D1 but not C0 cell extracts. The most significant hits included the GTP-binding cytoskeletal protein septin-9 (42), the serine-threonine kinase NDR1 (12), and the actin-binding protein filamin-B (35) (Table 1).

MICAL-1 interacts with NDR1 and NDR2 kinases. Since NDR kinases and MICALs display an intriguing overlap in their reported cellular functions (e.g., neurite growth/patterning and cytoskeletal dynamics [12, 18]), we focused our efforts in this study on understanding the role of MICAL-1/NDR interactions. First, the validity of the NDR1 mass spectrometry result was confirmed by Western blotting of independent pulldown samples from C0 and D1 cells with an NDR1-specific antibody. A prominent 55-kDa band was present specifically in

TABLE 1. Binding partners of MICAL-1 in stable L cells identified by mass spectrometry[a]

Protein	Mascot score	NCBI GI no.	Protein MM[b] (kDa)	No. of unique peptides
MICAL-1	1,956	46396473	116.7	264
Septin-9	554	56749655	65.5	12
NDR1	346	56749663	54.1	8
Filamin-B	318	38257404	277.6	8

[a] The table shows proteins identified with a significant Mascot score in pulldown experiments from D1 cell extracts. No peptides were identified for the indicated proteins in a parallel pulldown from C0 control cells.

[b] MM, molecular mass.

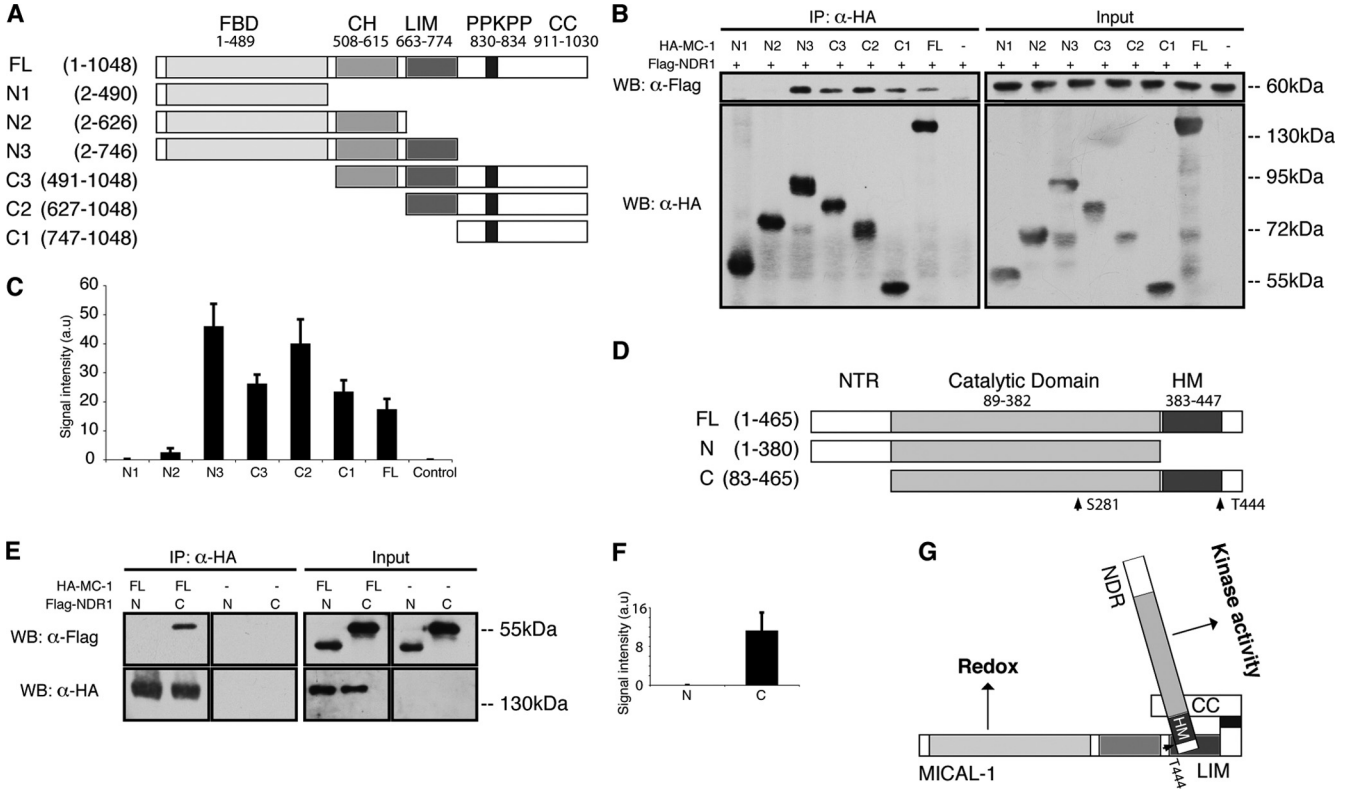

FIG. 2. MICAL-1 and NDR1 interact through domains involved in the regulation of their enzymatic activity. (A) Schematic representation of the domain structure of full-length (FL) mouse MICAL-1 and its truncation mutants. The numbers in parentheses and above the schematic representation are the amino acid positions. (B) Lysates of HEK293 cells transfected with Flag-NDR1 (+) and HA-tagged full-length or truncated MICAL-1 were immunoprecipitated (IP) with anti-HA antibody (α-HA) and analyzed by Western blotting (WB). (C) Microdensitometry of Flag-NDR1 coimmunoprecipitated with HA-MICAL-1 (full-length or truncation mutants) from three independent experiments similar to those shown in panel B. Signal intensity is shown in arbitrary units (a.u.). Values are means plus standard deviations (SD) (error bars). (D) Schematic depicting NDR1 and its truncation mutants with conserved domains indicated. The positions of the Ser281 and Thr444 regulatory phosphorylation sites are shown. HM, hydrophobic motif; NTR, N-terminal regulatory region. Numbers indicate amino acid positions. (E) Lysates of HEK293 cells transfected with HA-MICAL-1 and Flag-tagged full-length or truncated NDR1 were immunoprecipitated with anti-HA antibody and analyzed by Western blotting. (F) Microdensitometry of Flag-NDR1 coimmunoprecipitated with HA-MICAL-1 (+) from three independent experiments similar to those shown in panel E. Data are means plus SD. (G) Schematic of the identified interactions between MICAL-1 and NDR1. The LIM and C-terminal domains of MICAL-1 interact with the C-terminal region of NDR1 harboring the hydrophobic motif and the regulatory Thr444 phosphorylation site.

the D1 lane following anti-Flag pulldown (Fig. 1C). Immunoprecipitation experiments from HEK293 cells coexpressing myc-tagged MICAL-1 (myc-MICAL-1) and Flag-tagged NDR1 (Flag-NDR1) further confirmed the interaction of MICAL-1 with NDR1 (Fig. 1D). Using several of the available antibodies, we were unsuccessful in staining for endogenous NDR1 or NDR2 in cells (see also references 8 and 10). However, fluorescence microscopic analysis of COS-7 cells transfected with epitope-tagged MICAL-1 and NDR1 showed that the distribution of both proteins partially overlapped in the cytoplasm and in specific membrane regions (data not shown).

Two NDR kinases have been identified, NDR1 and NDR2 (12). NDR1 and NDR2 are ~87% identical at the amino acid level, and one of the peptides identified in our mass spectrometry analysis was shared between NDR1 and NDR2 (data not shown). It is therefore possible that MICAL-1 also binds to NDR2. To test this idea, HA-tagged MICAL-1 (HA-MICAL-1) and Flag-tagged NDR2 (Flag-NDR2) were coexpressed in HEK293 cells followed by pulldown with anti-Flag antibody. Indeed, HA-MICAL-1 coprecipitated with Flag-NDR2 (Fig. 1E). A similar result was obtained following coimmunoprecipitation of recombinant GST-NDR2 and HA-MICAL-1 protein purified from HEK293 cells (Fig. 1F). To determine whether the interaction between MICAL-1 and NDR1/2 was direct, the C-terminal region of MICAL-1 (C1; Fig. 2A) was purified from bacteria and used in a coimmunoprecipitation experiment with GST-NDR2. The ability of GST-NDR2 to coprecipitate MICAL-1 C1 indicates a direct interaction between NDR2 and the C-terminal region of MICAL-1 (Fig. 1G). Finally, we performed coimmunoprecipitation experiments from naïve L cell lysates using MICAL-1- and NDR-specific antibodies. Importantly, endogenous MICAL-1 coprecipitated with endogenous NDR1 and NDR2 and vice versa from naïve L cell extracts, indicating that in L cells endogenous MICAL-1/NDR1 complexes can be formed (Fig. 1H and data not shown).

MICAL-1 and NDR1 interact through domains involved in the regulation of their enzymatic activity. Both MICAL-1 and NDR1 are multidomain proteins. MICAL-1 contains an N-terminal flavoprotein monooxygenase (FM) domain, a calponin

homology domain, a LIM domain, proline-rich sequences, and coiled-coil motifs (Fig. 2A). NDR kinases contain an N-terminal regulatory (NTR) domain, a catalytic domain, and a C-terminal hydrophobic motif (HM) (Fig. 2D). To determine the domains required for MICAL-1/NDR1 interactions, a series of truncation mutants were generated for MICAL-1 (Fig. 2A) (28) and NDR1 (Fig. 2D) (10) and used in pulldown assays from HEK293 cells coexpressing mutants for MICAL-1 or NDR1 with full-length NDR1 or MICAL-1, respectively. Coprecipitation of endogenous MICAL-1 or NDR1 proteins was not detected in these experimental settings (data not shown). Intriguingly, constructs containing the LIM (N3, C3, and C2) and/or C-terminal domain (C3 to C1) of MICAL-1 showed binding to NDR1, indicating that both domains are required for association with NDR1 (Fig. 2B and C). Since intramolecular interactions between the LIM and C-terminal domains of MICAL-1 have been reported to enforce an autoinhibited protein conformation preventing flavoenzyme activity (28), this suggests that NDR1 might bind MICAL-1 in its autoinhibited state. Conversely, the NDR1 C-terminal region was required for interaction with MICAL-1 (Fig. 2E and F). This is intriguing because the NDR1 C-terminal region harbors the hydrophobic motif surrounding the Thr444 site, whose phosphorylation by MST kinases is required for full NDR1 kinase activity (23, 32, 38). In all, our results reveal an endogenous interaction between MICAL-1 and NDR1. Furthermore, NDR1 associates with two domains of MICAL-1 crucial for regulating its enzymatic activity, while reciprocally, MICAL-1 binds a region of NDR1 contributing to the control of NDR kinase activity (Fig. 2G).

MICAL-1 negatively regulates NDR1 kinase activation. To unveil the functional role of MICAL-1/NDR interactions, we first explored the idea that NDR kinases regulate MICAL-1. Thus far, two properties of MICAL-1 have been characterized in detail. First, MICAL-1 is an NADPH-dependent flavoprotein monooxygenase with redox activity (25, 30). Second, C-terminally truncated MICAL-1 proteins (N1 to N3 [Fig. 2A]) induce cell contraction in culture (28). This contraction response is most likely dependent on the FM domain and on redox activity, as mutagenesis of essential glycine residues in the MICAL-1 FM domain leads to loss of N1-induced cell contraction (data not shown). Intramolecular interactions between the LIM and C-terminal domains of MICAL-1 can inhibit FM activity (28). Because NDR1 associates with both domains, it is tempting to speculate that NDR kinases regulate MICAL-1 activity. To test this hypothesis, an enzyme-linked assay was used to determine the effect of NDR1/2 on MICAL-1 enzymatic activity based on H_2O_2 production (Fig. 3A and B) (25, 28). In line with previous observations, full-length (FL) MICAL-1 produced only low levels of H_2O_2, whereas constitutively active MICAL-1 N1-N3 truncation mutants showed high enzymatic activity (Fig. 3A to D) (25, 28). In a recent study, it was shown that cotransfection of the putative MICAL-1 substrate collapsin response mediator protein-2 (CRMP-2) with MICAL-1 in cells leads to a reduction in MICAL-1 N1-N3 H_2O_2 enzymatic activity. Similarly, recombinant GST-CRMP-2 induced a reduction in MICAL-1 N3 enzymatic activity (28). It was proposed that rather than producing H_2O_2, MICAL-1 may perform redox reactions on CRMP-2 in the presence of this substrate (28). In contrast to these findings, MICAL-1 activity was not inhibited by the cotransfection of NDR1 or by the addition of recombinant NDR2. Furthermore, NDR1/2 did not alter the enzymatic activity of FL MICAL-1 (Fig. 3C and D). In addition, shRNA-mediated knockdown of NDR1/2 in L cells did not affect the enzymatic activity of MICAL-1 N3 (Fig. 3E). Previous work has shown that cotransfection of FL MICAL-1 with CRMP-2 or plexin A1 induces COS-7 cell contraction (28). However, coexpression of NDR1/2 or a constitutively active form of NDR1 (NDR1-PIFtide [33]) with FL MICAL-1 did not induce cell contraction, and NDR1/2 overexpression or knockdown did not influence contraction triggered by N3 (Fig. 3F and G; also data not shown). These experimental results argue against a role for NDR1/2 in the control of MICAL-1 enzymatic and contraction activity. We next determined whether MICAL-1 could serve as a substrate for NDR kinases. Although we were able to establish that MICAL-1 is a phosphoprotein (Fig. 4A), GST-NDR2 failed to phosphorylate MICAL-1 in an *in vitro* kinase assay, indicating that MICAL-1 is not an NDR2 substrate (Fig. 4B). Unfortunately, production of GST-NDR1 protein is notoriously difficult, and we were unable to obtain sufficient quantities of NDR1 for kinase assays. In summary, our results strongly argue against a direct role for NDR1/2 in regulating MICAL-1 enzymatic activity and the subsequent cell morphological changes.

Therefore, we next examined whether MICAL-1 may regulate NDR kinases. Multisite phosphorylation is a general control mechanism of NDR1 and NDR2, which contain two main regulatory phosphorylation sites: Ser281/282 (NDR1/2, the activation segment) and Thr444/442 (the hydrophobic motif) (Fig. 2D). Upon MOB-1A binding to the N-terminal region, Ser281/282 is autophosphorylated, whereas Thr444/442 is targeted by upstream MST kinases (12). Treatment of cells with okadaic acid (OA), which preferentially inhibits protein phosphatase 2A, results in increased Ser281/282 and Thr444/442 phosphorylation and elevated NDR1/2 kinase activity (3, 32, 38). To study the potential effects of MICAL-1 on NDR1/2, we treated HEK293 cells transfected with Flag-NDR1 alone or in combination with HA-MICAL-1 with OA and assessed Ser281 and Thr444 phosphorylation of precipitated Flag-NDR1 protein using phospho-specific antibodies (Fig. 5A). Sixty minutes of OA treatment strongly induced Ser281 and Thr444 phosphorylation (data not shown). MICAL-1 overexpression did not influence OA-induced Ser281 autophosphorylation (Fig. 5A). Consistent with these data, we did not find an effect of MICAL-1 on GST-NDR2 autophosphorylation in kinase assays (Fig. 4B). It should be noted, however, that the currently available phosphorylated Ser281 (p-Ser281) antibody is not suitable for work with endogenous NDR kinases (unpublished data). In striking contrast, overexpression of HA-MICAL-1 drastically inhibited phosphorylation of Flag-NDR1 on Thr444 following OA treatment (Fig. 5A). This effect was dose dependent, as higher levels of HA-MICAL-1 were more efficient in lowering OA-induced NDR1 phosphorylation (Fig. 5B). Furthermore, MICAL-1 reduced Thr444 phosphorylation of endogenous NDR1 and NDR2 following OA treatment (Fig. 5C). It has been reported that at certain concentrations H_2O_2 can inhibit Thr444 phosphorylation (8). Since the MICAL-1 FM domain can produce H_2O_2 under specific conditions or potentially facilitate other redox reactions (Fig. 3) (25, 28), we

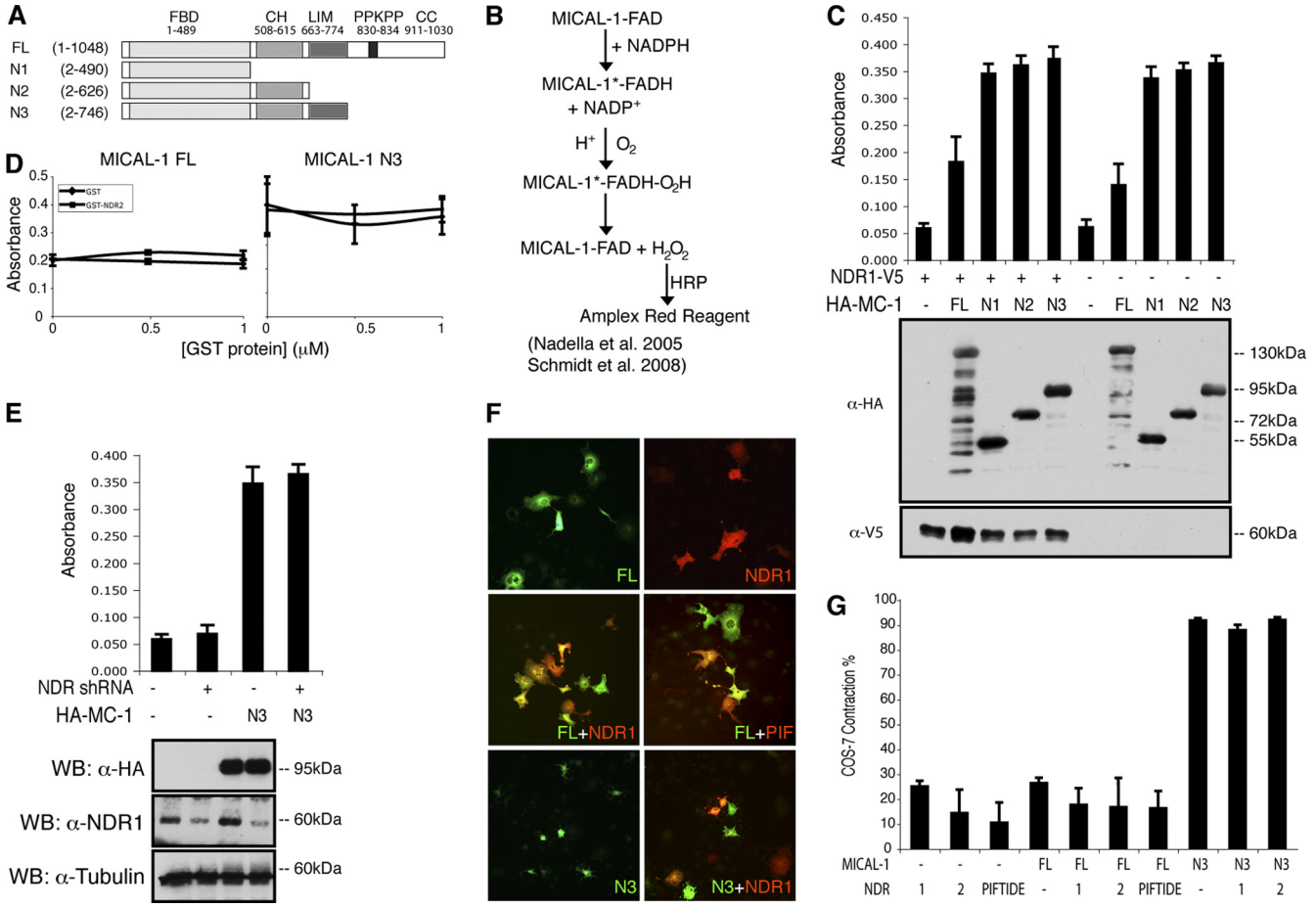

FIG. 3. NDR kinases have no effect on MICAL-1 enzymatic or cell contraction activity. (A) Schematic representation of the domain structure of full-length (FL) mouse MICAL-1 and truncation mutants used for H_2O_2 and COS-7 cell contraction assays. Numbers indicate amino acid positions. (B) Overview of the enzyme-linked assay used to determine H_2O_2 levels in two different experiments (see panels C and D) (25, 28). (C to E) Cell lysates (C and E) (28) and purified proteins (D) (25) were used to study MICAL-1 enzymatic activity in the presence (+) or absence (−) of NDR1/2 kinases. (C and E) Measurement of H_2O_2 production from lysates of HEK293 cells (C) or L cells (E) transfected with the indicated constructs in the presence of 200 μM NADPH. The gels below the graphs in panels C and E show a representative Western blot analysis of lysates used for enzymatic reactions. NDR shRNA targets NDR1 and NDR2. (D) Measurement of H_2O_2 production from purified full-length (FL) and truncated (N3) MICAL-1 proteins in the presence of different concentrations of GST or GST-NDR2. (F) COS-7 cells were transfected with the indicated MICAL-1 constructs alone or in combination with NDR1 (1), NDR2 (2), or NDR1-PIFtide (PIF). Transfected cells were immunostained with anti-GFP (MICAL-1; green) and anti-Flag (NDR1; red) antibodies. (G) Quantification of the cell contraction experiments shown in panel E (mean plus standard error of the mean [SEM] [error bar]). Cells with an area of ≤1,600 μm^2 were defined as contracted.

next asked whether MICAL-1 enzymatic activity mediates the negative effect of MICAL-1 on Thr444 phosphorylation. Site-directed mutagenesis was used to mutate the first FAD fingerprint in the MICAL-1 FM domain. These mutations disrupt FAD binding and block enzymatic activity without affecting the overall structure of the protein (19, 21, 44). MICAL-1 FL G3/W3 could, however, still reduce OA-induced Thr444 phosphorylation, suggesting that the inhibitory effect of MICAL-1 on Thr444 phosphorylation is independent of its enzymatic activity (Fig. 5C).

Next, to establish the physiological relevance of the MICAL-1 effect, the level of endogenous MICAL-1 in HEK293 cells was decreased by siRNA. In line with our previous results, knockdown of MICAL-1 resulted in an increased level of Thr444 phosphorylation triggered by OA compared to control (Fig. 5D). Thus, MICAL-1 is an endogenous negative regulator of NDR1 activation in HEK293 cells. Since phosphorylation of Thr444 is required for full kinase activity, we next examined the ability of MICAL-1 to reduce NDR1 kinase activity on NDR substrate peptide (Fig. 5E). Flag-NDR1 was expressed in HEK293 cells, alone or in combination with HA-MICAL-1, immunoprecipitated, and used in a peptide kinase assay. In line with its negative effect on Thr444 phosphorylation, MICAL-1 robustly inhibited NDR1 kinase activity, reducing peptide phosphorylation by about 40%. In conclusion, our results show that MICAL-1 is an endogenous negative regulator of NDR1 activation that inhibits T444 phosphorylation, thereby contributing to the control of NDR kinase activity.

MICAL-1 negatively regulates the activation of NDR1 kinase by competing with MST1 for NDR1 binding. Phosphorylation on Thr444/442 of NDR1 and NDR2 can be mediated by MST kinases (32, 40). MST1 can physically associate with the C-terminal hydrophobic motif of NDR1/2 and phosphorylate Thr444/442 upon activation by upstream signals such as

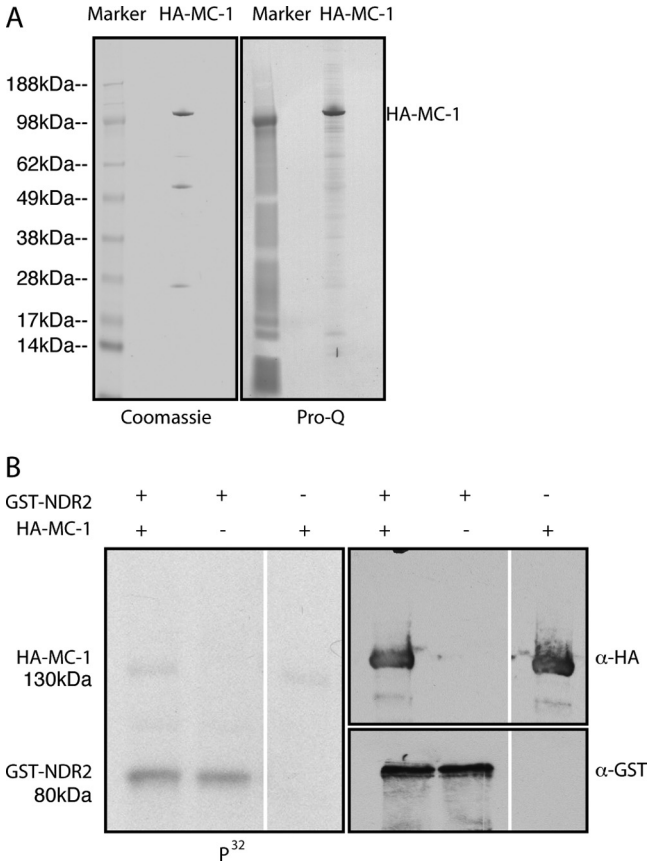

FIG. 4. MICAL-1 is a phosphoprotein but not a substrate of NDR2. (A) Lysates from HEK293 cells overexpressing HA-MICAL-1 were subjected to immunoprecipitation with anti-HA antibodies, separated on a gradient gel, and stained with Pro-Q phosphoprotein stain or with Coomassie blue to visualize all protein. The full-length form of mouse MICAL-1 is phosphorylated. Similar results were obtained with endogenous MICAL-1 protein precipitated from Neuro2A cells or brain lysate (data not shown). (B) HA-MICAL-1, immunoprecipitated from HEK293 cells, was used in an *in vitro* kinase assay with recombinant GST-NDR2. (Right) Western blotting was used to detect HA-MICAL-1 and GST-NDR2 input. MICAL-1 does not display increased phosphorylation in the presence of GST-NDR2. Conversely, NDR2 autophosphorylation (indicated by the 80-kDa bands) is unaffected by MICAL-1.

RASSF1A. MST1-induced NDR1/2 activation plays a crucial role downstream of RASSF1A in the apoptotic response to death receptor stimulation (40). Therefore, the association of MICAL-1 with the NDR C-terminal region and its ability to reduce Thr444 phosphorylation induced by OA invite the speculation that MICAL-1 regulates NDR kinase activation by interfering with the function of MST kinases. One possible mechanism could be that MICAL-1 associates with MST kinases and thereby controls their function. To test this model, we examined whether MICAL-1 can associate with MST1 following overexpression in cells. Although MST1 bound NDR1 (data not shown) (40), no interaction between MST1 and MICAL-1 was observed (Fig. 6A). Alternatively, MICAL-1 may serve as a substrate for MST1 competing with NDR kinases for phosphorylation. Therefore, the phosphorylation status of MICAL-1 was determined following shRNA-mediated knockdown of MST1 in cells. Interestingly, MICAL-1 phosphorylation was not affected by MST1 knockdown (Fig. 6B). To further test whether the regulation of NDR kinases by MICAL-1 involved the phosphorylation of MICAL-1 by MST1 kinase, we analyzed MICAL-1 as an MST1 substrate. This revealed that while kinase-dead NDR1 [NDR1(kd)] was strongly phosphorylated by recombinant MST1 (Fig. 6C, lane 5), purified MICAL-1 was not (Fig. 6C, lane 6), although MICAL-1 was present at higher abundance than NDR1. As expected, active MST1 also autophosphorylated itself (Fig. 6C, lanes 4 to 6), and all phosphorylation events were dependent on the presence of active MST1 (Fig. 6C, lanes 1 to 3). Notably, no effect of MICAL-1 expression on MST1 autophosphorylation was observed. Taken together, these findings suggest that MICAL-1 is not an MST1 substrate, arguing against the possibility that MICAL-1 interferes with phosphorylation of NDR by MST1 by serving as an alternative MST1 substrate.

A third possibility is that MICAL-1 competes with MST kinases for binding on the hydrophobic motif of NDR1. To test this idea, lysates from HEK293 cells expressing Flag-NDR1 and HA-MST1 were mixed with increasing amounts of lysates from HA-MICAL-1-expressing cells followed by anti-Flag immunoprecipitation. Increasing MICAL-1 levels led to a reduction in the amount of MST1 that coimmunoprecipitated with NDR1 despite similar MST1 input levels (Fig. 7A). As reported previously (11, 40), overexpression of MST1 leads to an increase in Thr444 phosphorylation (data not shown). To examine whether overexpression of MICAL-1 not only reduces MST1 binding but also causes a consequent decrease in MST1-induced Thr444 phosphorylation, we expressed HA-MST1 in combination with increasing amounts of HA-MICAL-1 and monitored Thr444 phosphorylation of endogenous NDR1/2. Indeed, MICAL-1 decreased MST1-induced Thr444 phosphorylation in a dose-dependent manner (Fig. 7B). In all, these results establish that MICAL-1 interferes with the binding of MST1 to NDR1/2, thereby negatively regulating MST1-induced NDR phosphorylation at the hydrophobic motif.

MICAL-1 interferes with apoptosis signaling. Since our findings indicate that MICAL-1 negatively regulates MST1-NDR signaling, we sought to determine whether MICAL-1 could affect a known biological function of the MST1-NDR pathway (40). The activation of NDR1/2 kinases through phosphorylation by MST1 is necessary for apoptosis signaling in mammalian cells (40). In addition, loss of NDR1/2 kinases can result in resistance to apoptosis (4). Therefore, wild-type L cells or stable C0 and D1 cells were treated for 12 h with vehicle or etoposide, a reagent known to induce apoptosis through NDR kinases (4), harvested, and analyzed by immunoblotting (Fig. 8A). Etoposide treatment triggered a robust increase in Thr444/442 phosphorylation in wild-type (not shown) and control (C0) cells concomitant with a strong induction of two apoptotic markers, i.e., cleaved PARP and cleaved caspase-3 (Fig. 8A). Furthermore, many cleaved caspase-3-positive C0 cells were detected following etoposide treatment (Fig. 8B). Intriguingly, etoposide exposure of D1 cells expressing MICAL-1-Flag/HA (Fig. 1) did not result in enhanced Thr444/442 phosphorylation (Fig. 8A). In line with this prominent inhibition of NDR activation, the signals for cleaved PARP and cleaved caspase-3 were dramatically lower in D1 cells than in control C0 cells following etoposide treat-

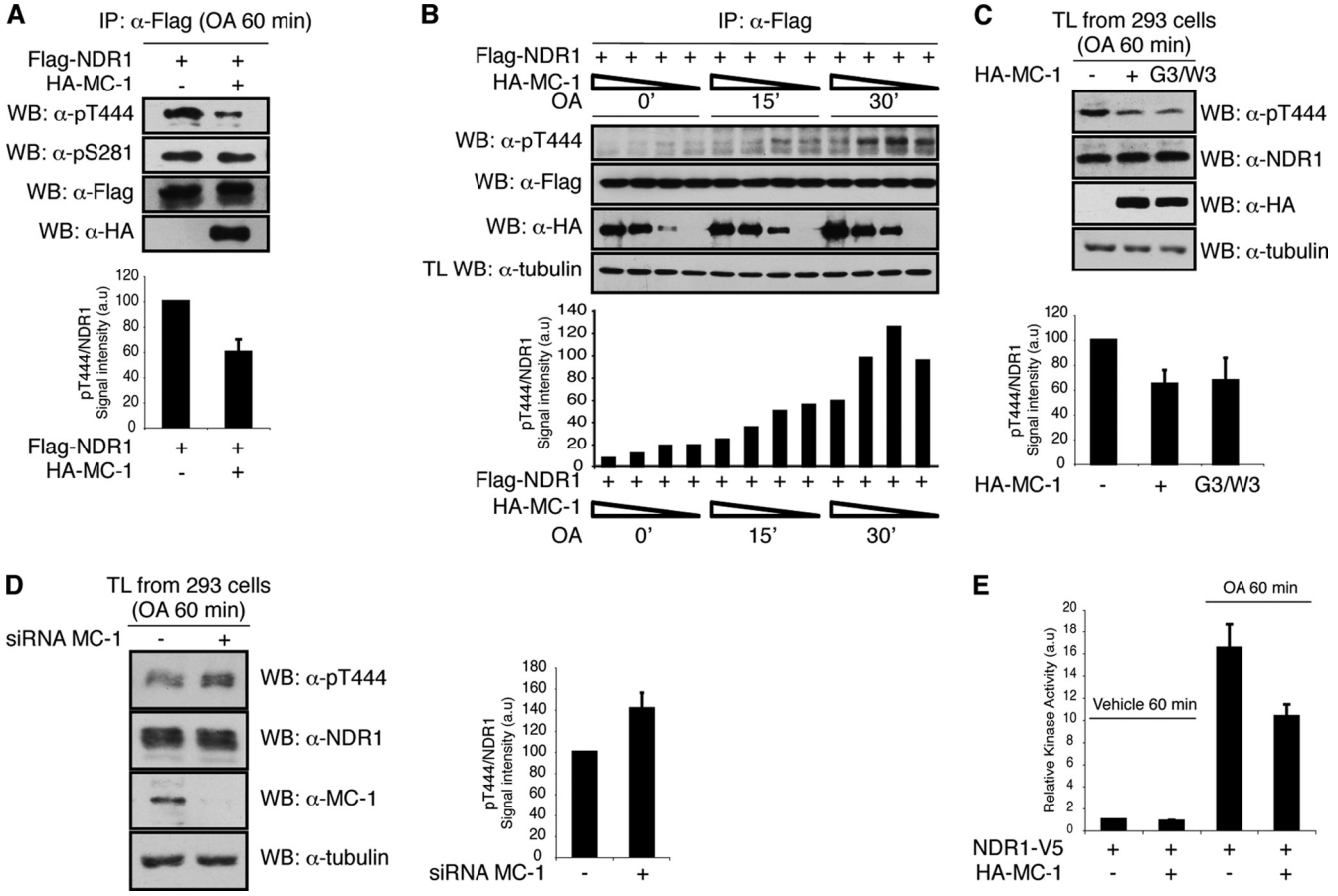

FIG. 5. MICAL-1 negatively regulates NDR1 kinase activation and activity. (A) HEK293 cells were transfected with Flag-NDR1 alone or in combination with HA-MICAL-1, treated with okadaic acid (OA) for 60 min and immunoprecipitated with anti-Flag antibody. Thr444 and Ser281 phosphorylation of precipitated NDR1 was assessed by Western blotting (WB) using phospho-specific antibodies (α-pT444, antibody against phosphorylated T4444). (Bottom) Microdensitometry from three independent experiments. Data are means plus SD (error bars). (B) HEK293 cells were transfected with Flag-NDR1 (+) in the absence or presence of different amounts of HA-MICAL-1 (the amount of HA-MICAL-1 is indicated by the height of the triangle above the lane) and treated with OA for the indicated periods of time (0 min [0′] to 30 min [30′]). Lysates were immunoprecipitated with anti-Flag antibodies, analyzed by Western blotting, and quantified (lower panel). The graph below the Western blots shows microdensitometry of a representative experiment. (C) HEK293 cells were transfected with pRK5 (−), HA-MICAL-1 (+), or HA-MICAL-1 G3/W3 (G3/W3) and treated with OA for 60 min, and total lysate (TL) was analyzed by Western blotting with the indicated antibodies. (Bottom) Microdensitometry from three independent experiments. Data are means plus SD. (D) HEK293 cells were transfected with a SMARTpool of ON-TARGETplus siRNAs against MICAL-1 (+) or with a pool of scrambled control siRNAs (−), treated with OA for 60 min, and then Western blotted with the indicated antibodies. The graph to the right of the Western blots shows microdensitometry from three independent experiments. Data are means plus SD. (E) HEK293 cells were transfected with V5-NDR1, alone or in combination with HA-MICAL-1, and treated with vehicle or OA. Immunoprecipitated V5-NDR1 protein was used for NDR peptide kinase assays. Data from a representative experiment with two replicate samples is shown. Error bars represent SDs.

ment (Fig. 8A), and only a few cleaved caspase-3-positive D1 cells were detected (Fig. 8B), suggesting that apoptotic signaling is inhibited in D1 cells. Similar results were obtained in a second, independent stable line expressing MICAL-1-Flag/HA (clone D2; not shown). In addition, the activation of NDR kinases (phosphorylated Thr444 [pThr444]) and cleavage of caspase-3 and PARP in response to TNF-α/CHX, another proapoptotic stimulus known to signal through NDR kinases (40), was reduced in D1 cells than in C0 cells (Fig. 8A). CHX alone did not induce apoptosis or affect pThr444 levels (40; also data not shown). Finally, to assess whether the inhibitory effect of MICAL-1 on apoptosis was dependent on its MO domain and redox signaling, we transiently transfected the constitutively active MICAL-1 N3 mutant or the FL MICAL-1 G3/W3 mutant into L cells and treated these cells with etoposide. Similar to FL MICAL-1, MICAL-1 G3/W3 reduced the etoposide-induced cleavage of caspase-3 (Fig. 8C). No effect of MICAL-1 N3 was observed. These results support the idea that the inhibitory effect of MICAL-1 on apoptosis is independent of its MO domain.

We also addressed the role of endogenous MICAL-1 in apoptosis regulation by RNA interference (RNAi). Wild-type L cells transfected with non-targeting control siRNAs or siRNAs specifically targeting mouse MICAL-1 were treated for 12 h with vehicle or etoposide, harvested, and analyzed by immunoblotting (Fig. 8D). In line with our biochemical and overexpression data, knockdown of MICAL-1 resulted in an increase in the overall amount of Thr444/442 phosphorylated

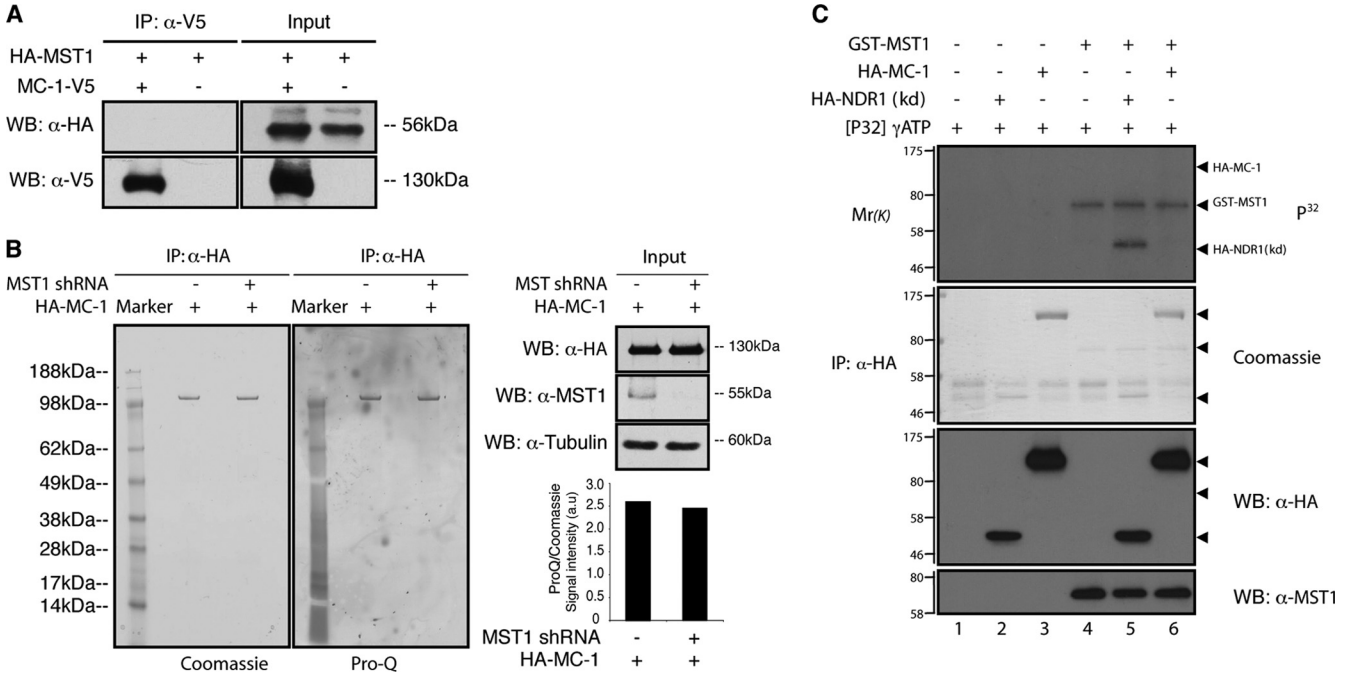

FIG. 6. MICAL-1 is not a substrate for MST1 kinase. (A) Lysates from HEK293 cells transfected with HA-MST1 alone or in combination with MC-1-V5 were immunoprecipitated with anti-V5 antibodies followed by Western blotting (WB). (B) Lysates of U2OS T-Rex cells were transfected with HA-MC-1 and treated with vehicle (−) or tetracycline (+) to induce MST1 shRNA expression. The lysates were subjected to immunoprecipitation with anti-HA antibodies followed by Coomassie blue or Pro-Q staining or WB with the indicated antibodies. The graph shows microdensitometry from a representative experiment. (C) Lysates of COS-7 cells transiently expressing empty vector, HA-NDR1 kinase-dead [HA-DNR1(kd)], or HA-MC-1 were subjected to immunoprecipitation with anti-HA antibody. Immunopurified proteins were then processed for kinase assays without or with GST-MST1. The proteins were then separated by SDS-PAGE and visualized either by autoradiography (top panel) or Coomassie blue staining. In parallel, samples were analyzed by Western blotting using anti-HA and anti-MST1 antibodies. The positions of HA-MC-1, GST-MST1, and HA-NDR1 (in kilodaltons) are indicated by arrowheads to the right of the Western blots. The relative molecular weights (Mr) (in thousands [*K*]) are indicated to the left of the Western blots.

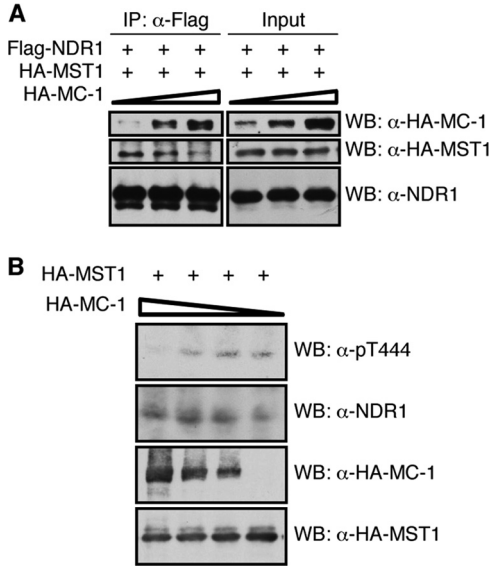

FIG. 7. MICAL-1 competes with MST1 for NDR1 binding. (A) Lysates from HEK293 cells transfected with Flag-NDR1, HA-MST1, or HA-MICAL-1 were mixed as indicated, immunoprecipitated with anti-Flag antibodies, and analyzed by Western blotting (WB). (B) HEK293 cells were transfected with HA-MST1 in the presence of different amounts of HA-MICAL-1. Lysates were subjected to WB with the indicated antibodies.

NDR and in increased signals for cleaved PARP and cleaved caspase-3 (Fig. 8D). Although etoposide and TNF-α can induce apoptosis through the MST1-NDR pathway, it is formally possible that the observed effects of MICAL-1 on apoptosis do not involve modulation of NDR signaling. To address this point, L cells were transiently transfected with siRNAs targeting MICAL-1, shRNA constructs targeting NDR1/2 or combinations thereof, followed by etoposide treatment. Knockdown of MICAL-1 led to increased signals for cleaved caspase-3, while as shown previously (4), knockdown of NDR1/2 inhibited the cleavage of caspase-3 induced by etoposide (Fig. 8E). Interestingly, following simultaneous knockdown of MICAL-1 and NDR1/2, no induction of caspase-3 cleavage was observed, indicating that MICAL-1 and NDR1/2 function in the same pathway. In all, we conclude that MICAL-1 has inhibitory effects on proapoptotic signaling through the NDR-MST pathway.

DISCUSSION

Phosphorylation of NDR1/2 kinases by MST1 is required for full NDR kinase activity and for the induction of apoptosis in response to proapoptotic stimuli (4, 40). The deregulation of NDR1 and MST kinases predisposes the organism to the development of cancer due to compromised apoptotic responses (4, 31). Despite the critical role of MST-induced NDR phos-

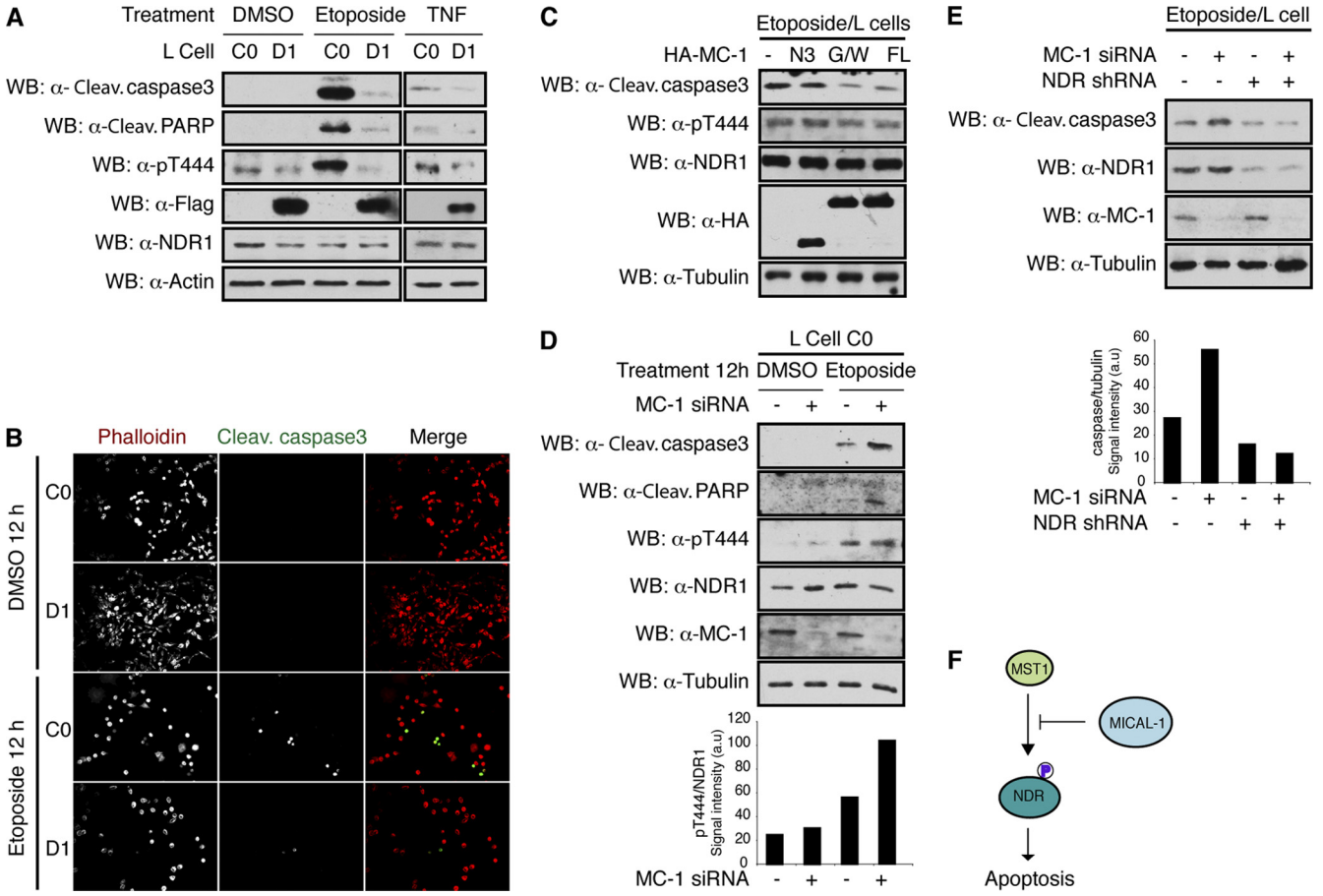

FIG. 8. MICAL-1 inhibits NDR-dependent apoptotic signaling. (A) Stable C0 and D1 L cells were treated with control compound (DMSO or CHX [not shown]), etoposide, or TNF-α/CHX (4, 40). Lysates were processed for Western blotting using the indicated antibodies. Cleav., cleaved. (B) Stable C0 and D1 L cells were treated as described above for panel A and immunostained using phalloidin-TRITC (red) to visualize cell morphology and anti-cleaved caspase-3 (green) antibody. (C) L cells were transiently transfected with empty vector or constructs for FL MICAL-1, FL MICAL-1 G3/W3, or MICAL-1 N3, treated with etoposide, and processed for Western blotting using the indicated antibodies. (D) L cells were transfected with non-targeting control siRNA (−) or with siRNA oligonucleotides targeting mouse MICAL-1 (+), treated as described above for panel A, and processed for Western blotting using the indicated antibodies. The graph shows a quantification of the levels in the Western blots. (E) L cells were transfected with non-targeting control siRNA or shRNA (−), siRNA oligonucleotides targeting mouse MICAL-1 (+), shRNA constructs targeting NDR1/2, or combinations thereof, treated as described above for panel A, and processed for Western blotting using the indicated antibodies. The graph shows a quantification of the levels in the Western blots. (F) Schematic representation of the inhibitory role of MICAL-1 in the MST1-NDR signaling pathway during apoptosis. P, phosphate.

phorylation in different cell biological processes and in disease, it has remained unknown if or how this key phosphorylation event is regulated. Our findings identify MICAL-1 as a novel endogenous negative regulator of MST1-NDR signaling and apoptosis in mammalian cells (Fig. 8F). MICAL-1 specifically and endogenously interacts with the hydrophobic motif of NDR1/2 (Fig. 1 and 2) and colocalizes with NDR1 in cells, and ectopic expression of MICAL-1 reduces NDR kinase activation and activity (Fig. 5). Knockdown of endogenous MICAL-1, on the other hand, results in increased NDR kinase phosphorylation (Fig. 5). Furthermore, we found that MICAL-1 does not bind MST1 or serve as a MST1 substrate (Fig. 6) but competes with MST1 for NDR binding (Fig. 7) and thereby reduces MST1-induced NDR activation (Fig. 7). In line with this inhibitory effect, overexpression and knockdown studies show that MICAL-1 negatively affects a known biological function of the MST1-NDR1/2 pathway, namely, proapoptotic signaling (Fig. 8). Together, these results uncover a novel and unique regulatory mechanism of MST-NDR signaling.

Binding of MOB1 to the N-terminal region of NDR1/2 stimulates autophosphorylation and NDR activation (3). Kohler and colleagues recently reported that human MOB2 (hMOB2) can act as an inhibitor of hMOB1-NDR signaling by competing with hMOB1 for binding to the N-terminal domain of NDR1/2 (16). Here we describe an unexpected additional level of NDR regulation. By competing with MST1 for binding to the C-terminal hydrophobic motif domain, MICAL-1 can regulate NDR1/2 activation (Fig. 8F). Together, these studies define a novel level of NDR kinase regulation through competitive inhibitors that directly interfere with the binding of key upstream activating signals, such as MOB1 and MST1. How these competitive inhibitors are controlled is unknown. It is possible that previously identified MICAL-1 interactors such as plexin

proteins contribute to this regulation. Plexins function as evolutionary conserved type I transmembrane receptors for semaphorin proteins in different cell types and organ systems and mediate diverse cellular processes, including apoptosis (7, 27, 46). For example, semaphorin 3A can induce neuron or leukemic cell death through plexin A3 and plexin A1, respectively (1, 24). Intriguingly, MICAL-1 can associate with the cytoplasmic domains of the four class A plexins, and semaphorin ligand stimulation enhances this interaction (28) (Y. Zhou and R. J. Pasterkamp, unpublished observations). Recruitment of MICAL-1 to plexin upon ligand stimulation may reduce the availability of MICAL-1 for inhibiting MST-induced NDR activation, leading to enhanced NDR activity and apoptosis. Alternatively, the regulation of MICAL-1 activity by upstream signaling cues such as protein kinases may be crucial for controlling its inhibitory role in the MST-NDR pathway. This idea gains support from the observation that MICAL-1 is phosphorylated in cells and neural tissues (Fig. 4A), suggesting that it is a substrate for upstream kinases. Future studies will address these and other possible mechanisms.

It is plausible that the MICAL-1-dependent regulatory mechanism delineated in this study also functions in MST- and/or NDR-dependent cellular processes other than apoptosis. For example, the MST1-NDR pathway was recently implicated in the control of centrosome duplication (11). Furthermore, striking similarities exist between the effects of manipulating MST, MICAL, and NDR on neuronal morphology. Knockdown of MST3b or overexpression of constitutively active MICAL-1 in cultured mammalian neurons reduces neurite growth (14, 28), while exogenous NDR2 expression enhances neurite growth (34). The loss of *Tricornered* (NDR) or *Hippo* (MST) in *Drosophila* and the loss of *SAX-1* (NDR) in *Caenorhabditis elegans* leads to altered dendritic arborization and tiling defects (i.e., ectopic overlap between individual dendritic trees) (5, 6, 9). Loss of *Drosophila Mical* also results in enlarged dendritic fields due to deficits in dendritic pruning (15). These observations together with our own findings support a model in which MST, MICAL, and NDR are components of a common molecular pathway that controls the formation and remodeling of the initial imprecise neuronal network into functional neuronal connections.

In the present study, no effect of NDR1/2 on MICAL-1 enzymatic activity or cell contraction was detected, but it is possible that NDR1/2 influences other proposed MICAL effects such as on Rab-mediated vesicle transport (41) or myofilament organization (2). It is also interesting to note that knockdown of MST3b leads to a reduction in CRMP-1, a putative substrate for the MICAL-1 flavoprotein monooxygenase domain (14, 28). Thus, MICAL-1 may not only negatively regulate MST kinases, but MSTs might also influence MICAL-1 function by controlling its substrate levels.

Taking all the results of this study together, this study reveals a previously unknown biological role for MICAL-1 in apoptosis and defines a novel negative regulatory mechanism of MST-NDR signaling. Future experiments are needed to decipher the precise role of MICAL-1 in the activation of NDR kinases by extrinsic and intrinsic apoptotic stimuli. Further elucidation of the role of MICAL-1 in MST-NDR signaling can be expected to open new avenues for the molecular delineation of MST/NDR functioning in different cell biological processes and for understanding how deregulation of this pathway contributes to disease.

ACKNOWLEDGMENTS

We thank Dianne van den Heuvel for providing the plexinA4Δecto construct and Jeroen den Hertog and Peter Burbach for helpful comments on the manuscript. Anti-T442/444-P and anti-S281/282-P antibodies were kindly provided by Brian Hemmings (FMI, Basel, Switzerland).

This work was supported by The Netherlands Organization for Health Research and Development (ZonMW-VIDI and ZonMW-TOP), the Human Frontier Science Program (HFSP-CDA), and the Genomics Center Utrecht (to R.J.P.), the Fondation Leducq and the British Heart Foundation (to P.H.S and S.J.F.), and the European Seventh Framework Programme under grant agreement Health-2009-2.1.2-1-242167 (SynSys project, to A.B.S., R.C.V.D.S., and K.W.L.). A.H. is supported by a Wellcome Trust Career Development Research Fellowship.

REFERENCES

1. **Ben-Zvi, A., et al.** 2008. The Semaphorin receptor PlexinA3 mediates neuronal apoptosis during dorsal root ganglia development. J. Neurosci. **28:** 12427–12432.
2. **Beuchle, D., H. Schwarz, M. Langegger, I. Koch, and H. Aberle.** 2007. Drosophila MICAL regulates myofilament organization and synaptic structure. Mech. Dev. **124:**390–406.
3. **Bichsel, S. J., R. Tamaskovic, M. R. Stegert, and B. A. Hemmings.** 2004. Mechanism of activation of NDR (nuclear Dbf2-related) protein kinase by the hMOB1 protein. J. Biol. Chem. **279:**35228–35235.
4. **Cornils, H., et al.** 2010. Ablation of the kinase NDR1 predisposes mice to the development of T cell lymphoma. Sci. Signal. **3:**ra47.
5. **Emoto, K., et al.** 2004. Control of dendritic branching and tiling by the Tricornered-kinase/Furry signaling pathway in Drosophila sensory neurons. Cell **119:**245–256.
6. **Emoto, K., J. Z. Parrish, L. Y. Jan, and Y. N. Jan.** 2006. The tumour suppressor Hippo acts with the NDR kinases in dendritic tiling and maintenance. Nature **443:**210–213.
7. **Franco, M., and L. Tamagnone.** 2008. Tyrosine phosphorylation in semaphorin signalling: shifting into overdrive. EMBO Rep. **9:**865–871.
8. **Fuller, S. J., et al.** 2008. Nuclear Dbf2-related protein kinases (NDRs) in isolated cardiac myocytes and the myocardium: activation by cellular stresses and by phosphoprotein serine-/threonine-phosphatase inhibitors. Cell Signal. **20:**1564–1577.
9. **Gallegos, M. E., and C. I. Bargmann.** 2004. Mechanosensory neurite termination and tiling depend on SAX-2 and the SAX-1 kinase. Neuron **44:**239–249.
10. **Hergovich, A., S. J. Bichsel, and B. A. Hemmings.** 2005. Human NDR kinases are rapidly activated by MOB proteins through recruitment to the plasma membrane and phosphorylation. Mol. Cell. Biol. **25:**8259–8272.
11. **Hergovich, A., et al.** 2009. The MST1 and hMOB1 tumor suppressors control human centrosome duplication by regulating NDR kinase phosphorylation. Curr. Biol. **19:**1692–1702.
12. **Hergovich, A., M. R. Stegert, D. Schmitz, and B. A. Hemmings.** 2006. NDR kinases regulate essential cell processes from yeast to humans. Nat. Rev. Mol. Cell Biol. **7:**253–264.
13. **Hung, R. J., et al.** 2010. Mical links semaphorins to F-actin disassembly. Nature **463:**823–827.
14. **Irwin, N., Y. M. Li, J. E. O'Toole, and L. I. Benowitz.** 2006. Mst3b, a purine-sensitive Ste20-like protein kinase, regulates axon outgrowth. Proc. Natl. Acad. Sci. U. S. A. **103:**18320–18325.
15. **Kirilly, D., et al.** 2009. A genetic pathway composed of Sox14 and Mical governs severing of dendrites during pruning. Nat. Neurosci. **12:**1497–1505.
16. **Kohler, R. S., D. Schmitz, H. Cornils, B. A. Hemmings, and A. Hergovich.**2010. Differential NDR/LATS interactions with the human MOB family reveal a negative role for human MOB2 in the regulation of human NDR kinases. Mol. Cell. Biol. **30:**4507–4520.
17. **Kolk, S. M., et al.** 2009. Semaphorin 3F is a bifunctional guidance cue for dopaminergic axons and controls their fasciculation, channeling, rostral growth, and intracortical targeting. J. Neurosci. **29:**12542–12557.
18. **Kolk, S. M., and R. J. Pasterkamp.** 2007. MICAL flavoprotein monooxygenases: structure, function and role in semaphorin signaling. Adv. Exp. Med. Biol. **600:**38–51.
19. **Kubo, A., S. Itoh, K. Itoh, and T. Kamataki.** 1997. Determination of FAD-binding domain in flavin-containing monooxygenase 1 (FMO1). Arch. Biochem. Biophys. **345:**271–277.
20. **Lahiry, P., A. Torkamani, N. J. Schork, and R. A. Hegele.** 2010. Kinase mutations in human disease: interpreting genotype-phenotype relationships. Nat. Rev. Genet. **11:**60–74.

21. **Lawton, M. P., and R. M. Philpot.** 1993. Functional characterization of flavin-containing monooxygenase 1B1 expressed in Saccharomyces cerevisiae and Escherichia coli and analysis of proposed FAD- and membrane-binding domains. J. Biol. Chem. **268:**5728–5734.
22. **Li, K. W., et al.** 2007. Quantitative proteomics and protein network analysis of hippocampal synapses of CaMKIIalpha mutant mice. J. Proteome Res. **6:**3127–3133.
23. **Millward, T. A., D. Hess, and B. A. Hemmings.** 1999. Ndr protein kinase is regulated by phosphorylation on two conserved sequence motifs. J. Biol. Chem. **274:**33847–33850.
24. **Moretti, S., et al.** 2008. Semaphorin3A signaling controls Fas (CD95)-mediated apoptosis by promoting Fas translocation into lipid rafts. Blood **111:** 2290–2299.
25. **Nadella, M., M. A. Bianchet, S. B. Gabelli, J. Barrila, and L. M. Amzel.** 2005. Structure and activity of the axon guidance protein MICAL. Proc. Natl. Acad. Sci. U. S. A. **102:**16830–16835.
26. **Pasterkamp, R. J., et al.** 2006. MICAL flavoprotein monooxygenases: expression during neural development and following spinal cord injuries in the rat. Mol. Cell Neurosci. **31:**52–69.
27. **Pasterkamp, R. J., and R. J. Giger.** 2009. Semaphorin function in neural plasticity and disease. Curr. Opin. Neurobiol. **19:**263–274.
28. **Schmidt, E. F., S. O. Shim, and S. M. Strittmatter.** 2008. Release of MICAL autoinhibition by semaphorin-plexin signaling promotes interaction with collapsin response mediator protein. J. Neurosci. **28:**2287–2297.
29. **Shevchenko, A., M. Wilm, O. Vorm, and M. Mann.** 1996. Mass spectrometric sequencing of proteins from silver-stained polyacrylamide gels. Anal. Chem. **68:**850–858.
30. **Siebold, C., et al.** 2005. High-resolution structure of the catalytic region of MICAL (molecule interacting with CasL), a multidomain flavoenzyme-signaling molecule. Proc. Natl. Acad. Sci. U. S. A. **102:**16836–16841.
31. **Song, H., et al.** 2010. Mammalian Mst1 and Mst2 kinases play essential roles in organ size control and tumor suppression. Proc. Natl. Acad. Sci. U. S. A. **107:**1431–1436.
32. **Stegert, M. R., A. Hergovich, R. Tamaskovic, S. J. Bichsel, and B. A. Hemmings.** 2005. Regulation of NDR protein kinase by hydrophobic motif phosphorylation mediated by the mammalian Ste20-like kinase MST3. Mol. Cell. Biol. **25:**11019–11029.
33. **Stegert, M. R., R. Tamaskovic, S. J. Bichsel, A. Hergovich, and B. A. Hemmings.** 2004. Regulation of NDR2 protein kinase by multi-site phosphorylation and the S100B calcium-binding protein. J. Biol. Chem. **279:**23806–23812.
34. **Stork, O., et al.** 2004. Neuronal functions of the novel serine/threonine kinase Ndr2. J. Biol. Chem. **279:**45773–45781.
35. **Stossel, T. P.** 2010. Filamins and the potential of complexity. Cell Cycle **9:**1463.
36. **Suto, F., et al.** 2005. Plexin-a4 mediates axon-repulsive activities of both secreted and transmembrane semaphorins and plays roles in nerve fiber guidance. J. Neurosci. **25:**3628–3637.
37. **Suzuki, T., et al.** 2002. MICAL, a novel CasL interacting molecule, associates with vimentin. J. Biol. Chem. **277:**14933–14941.
38. **Tamaskovic, R., S. J. Bichsel, H. Rogniaux, M. R. Stegert, and B. A. Hemmings.** 2003. Mechanism of Ca2+-mediated regulation of NDR protein kinase through autophosphorylation and phosphorylation by an upstream kinase. J. Biol. Chem. **278:**6710–6718.
39. **Terman, J. R., T. Mao, R. J. Pasterkamp, H. H. Yu, and A. L. Kolodkin.** 2002. MICALs, a family of conserved flavoprotein oxidoreductases, function in plexin-mediated axonal repulsion. Cell **109:**887–900.
40. **Vichalkovski, A., et al.** 2008. NDR kinase is activated by RASSF1A/MST1 in response to Fas receptor stimulation and promotes apoptosis. Curr. Biol. **18:**1889–1895.
41. **Weide, T., J. Teuber, M. Bayer, and A. Barnekow.** 2003. MICAL-1 isoforms, novel rab1 interacting proteins. Biochem. Biophys. Res. Commun. **306:**79–86.
42. **Weirich, C. S., J. P. Erzberger, and Y. Barral.** 2008. The septin family of GTPases: architecture and dynamics. Nat. Rev. Mol. Cell Biol. **9:**478–489.
43. **Wessel, D., and U. I. Flugge.** 1984. A method for the quantitative recovery of protein in dilute solution in the presence of detergents and lipids. Anal. Biochem. **138:**141–143.
44. **Wierenga, R. K., P. Terpstra, and W. G. Hol.** 1986. Prediction of the occurrence of the ADP-binding beta alpha beta-fold in proteins, using an amino acid sequence fingerprint. J. Mol. Biol. **187:**101–107.
45. **Zhao, B., L. Li, Q. Lei, and K. L. Guan.** 2010. The Hippo-YAP pathway in organ size control and tumorigenesis: an updated version. Genes Dev. **24:** 862–874.
46. **Zhou, Y., R. A. Gunput, and R. J. Pasterkamp.** 2008. Semaphorin signaling: progress made and promises ahead. Trends Biochem. Sci. **33:**161–170.